Mat. Res. Soc. Symp. Proc. Vol. 664 © 2001 Materials Research Society

Structural Characterization of SiF_4, SiH_4 and H_2 Hot-Wire-Grown Microcrystalline Silicon Thin Films with Large Grains

J. J. Gutierrez, C. E. Inglefield, C. P. An[1], M. C. DeLong[1], P. C. Taylor[1], S. Morrison[2], A. Madan[2]
Department of Physics, Weber State University
Ogden, UT 84408, U.S.A.
[1]Department of Physics, University of Utah
Salt Lake City, UT 84112, U.S.A.
[2]MVSystems
Golden, CO 80401, U.S.A.

ABSTRACT

In this paper, we present a comprehensive study of microcrystalline silicon thin film samples deposited by a novel growth process intended to maximize their grain size and crystal volume fraction. Using Atomic Force Microscopy, Raman spectroscopy, and x ray diffraction the structural properties of these samples were characterized qualitatively and quantitatively. Samples were grown using a Hot-Wire Chemical Vapor Deposition process with or without a post-growth hot-wire annealing treatment. During Hot-Wire Chemical Vapor Deposition, SiF_4 is used along with SiH_4 and H_2 to grow the thin films. After growth, some samples received an annealing treatment with only SiF_4 and H_2 present. These samples were compared to each other in order to determine the deposition conditions that maximize grain size. Large microcrystalline grains were found to be aggregates of much smaller crystallites whose size is nearly independent of deposition type and post-annealing treatment. Thin films deposited using the deposition process with SiF_4 partial flow rate of 2 sccm and post-growth annealing treatment had the largest aggregate grains ~ .5 μm and relatively high crystal volume fraction.

INTRODUCTION

The need to improve the performance of large-area electronic devices such as thin film transistors (TFT) and solar cells has motivated research interest in microcrystalline silicon thin films (μc-Si) and Hot-Wire Chemical Vapor Deposition (HWCVD). There are potential advantages to using μc-Si instead of hydrogenated amorphous silicon thin films (a-Si:H) in these applications. The μc-Si thin films have superior doping efficiency, higher carrier mobility, and lower dark conductivity [1-3]. In addition, μc-Si films have a lower hydrogen content which improves stability against light induced degradation known as the Staebler-Wronski effect [4, 5]. The details of the deposition technique affect the quality of μc-Si thin film. The use of HWCVD has been found to improve the quality of thin films compared to those grown by glow-discharge techniques [6].

The quality of a μc-Si thin film is often determined by its structural properties. Grain size and crystal volume fraction (x_c) affect fundamental electronic properties that have a significant effect on device performance. Consequentially, maximizing grain size

and crystal volume fraction leads to better thin film devices [7]. Our attempt to maximize grain size and crystal volume fraction has focused upon a novel technique combining HWCVD with a post-growth treatment. In our procedure, SiF_4 is added as a source gas along with H_2-diluted SiH_4 during growth using a tantalum filament. Afterwards, the thin films receive a post-growth annealing treatment with only SiF_4 and H_2 present. Using SiF_4 and H_2 in such a manner has been shown in PECVD to increase both x_c and grain size [8-11].

In this paper, we present a comprehensive study of the structural properties of the μc-Si thin films grown by the HWCVD technique with different deposition conditions. X ray diffraction, Raman spectroscopy, and Atomic Force Microscopy (AFM) are used to characterize qualitatively and quantitatively the structural properties of all samples. These techniques have been shown previously to provide complementary information [12]. A discussion of the results shows how grain size and crystalline volume fraction improves through the use of this novel technique.

EXPERIMENTAL DETAILS

All μc-Si thin film samples were grown on a 1737 glass substrate using a MVSystems HWCVD deposition chamber. All substrates were heated to a temperature (T_s) of 300°C and placed (l) 5 cm from a tantalum filament. The filament temperature (T_f) during deposition was measured by optical pyrometry to be 1880-1900°C. From a large set of samples, we chose four representative samples for discussion. The four sample designations and growth flow rates (F_x) referred to in the discussion of this paper are listed in Table 1. Samples that received a post-growth treatment were subject to an annealing with the following deposition conditions: T_f = 1880-1900°C, T_s = 300°C, l = 5 cm, F_{H2} = 80 sccm and F_{SiF4} = 1 sccm.

X ray diffraction measurements were performed in a standard powder apparatus. The broadening of the x ray peaks was used to calculate crystallite size (l_c) in the <111>, <220>, and <311> directions using the Debye-Sherrer formula [12]. The microcrystalline Raman spectra were fit to a sum of two Lorentzian peaks corresponding to the crystalline and amorphous phases. This allows us to calculate the crystalline volume fraction (x_c) from a ratio of the integrated peak intensities and average distance between point defects (l_d) from the full-width half maximum (FWHM) of the crystalline peak [13-15]. The

Table 1. Summary of deposition conditions discussed in paper. Treatment refers to the post-growth annealing.

Sample	**Treatment Applied**	**Flow Rate for SiH_4 (F_{SiH4})**	**Flow Rate for H_2 (F_{H2})**	**Flow Rate for SiF_4 (F_{SiF4})**
A	Yes	2 sccm	80 sccm	2 sccm
B	No	2 sccm	80 sccm	2 sccm
C	Yes	2 sccm	80 sccm	1 sccm
D	No	2 sccm	80 sccm	1 sccm

apparatus used to gather the Raman spectra is composed of an Argon ion laser with a wavelength of 514.5 nm with a power of 300 mW, collection optics, 0.6 m triple monochromator, and a cooled CCD camera. The background signal as measured by the CCD detector was subtracted from the Raman spectra. To image the surface topology of the thin films a model Topometrix TMX 2000 Scanning Probe Microscope in contact mode with a pyramidal tip was used for AFM. Imaging software is used to level the image by a nonlinear least-squares fit algorithm. The software also filtered selected noise frequencies out of the image using a 2D Fast Fourier Transform (FFT).

RESULTS AND DISCUSSION

The results of the Raman spectroscopy and x ray diffraction experiment are listed in Figure 1 and Table 2. AFM images for each sample are shown in Figure 2. Figure 1 shows typical Raman spectra gathered for crystalline silicon (c-Si), a-Si, and μc-Si. In Table 2, the data for Raman c-Si and a-Si are included for comparison. The peak frequency (ω_o) and FWHM values refer to a two peak fit of the Raman spectra for μc-Si. From the FWHM of the Raman crystalline peak l_d is derived; the area beneath the crystalline and amorphous peak are used to calculate the crystal volume [14,15].

In previous studies, Raman data gathered for microcrystalline silicon show that there is a maximum detection threshold for x_c around 0.70 [14, 15]. This indicates that there is a point at which the amorphous peak becomes too small to make an accurate measurement because it becomes lost in instrumentation noise. Thus, the samples in this study are approaching the limiting value of x_c that can be measured by Raman spectroscopy (see Table 2).

Figure 1. Typical Raman spectra for c-Si, a-Si, and μc-Si.

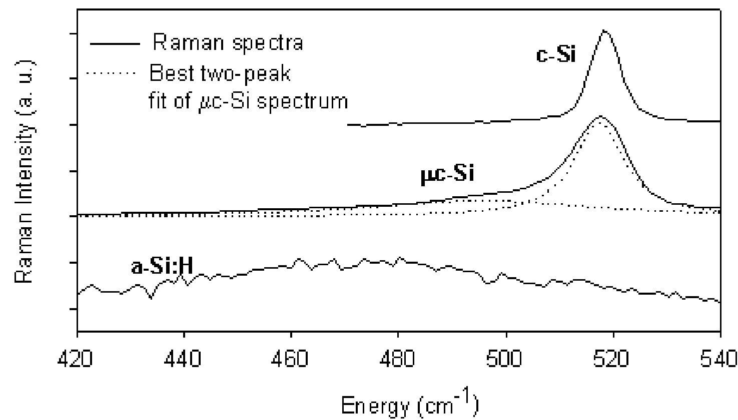

From the AFM and Raman spectroscopy data (see Figure 2 and Table 2), two trends are observed: the application of the post-growth treatment increases both grain size (l_g) measured by AFM and perhaps x_c. Grain sizes in Sample A, where the post growth treatment was applied, are much larger than the samples that either did not receive the treatment (B,D) or used a lower F_{SiF4} during deposition (C). Among the deposition conditions for Sample A, the parameter that maximizes post-growth treatment grain size is found to be the F_{SiF4} = 2 sccm. This observation correlates with a large x_c and l_d also observed for Sample A (see Table 2). The uncertainty in x_c from the fits included in Table 2 refers to relative comparisons between the samples. Systematic errors could

Table 2. A summary of x ray diffraction, Raman spectroscopy, and AFM results discussed in this paper. Some values for c-Si and a-Si are included for reference.

Sample	**l_c (± 40Å)**	**X-tal Peak ω_o (cm^{-1})**	**X-tal Peak FWHM (cm^{-1})**	**Amor. Peak ω_o (cm^{-1})**	**Amor. Peak FWHM (cm^{-1})**	**l_d (± 5Å)**	**x_c (± 4)**	**l_g (µm)**
c-Si	-	518.5	6.2	-	-	80	1.00	-
A	330	511.0	13.1	499.0	27.0	48.0	0.65	~0.5
B	280	510.0	13.3	491.0	46.0	48.0	0.61	~0.3
C	460	517.0	16.3	489.0	59.6	41.0	0.55	~0.1
D	340	512.0	15.7	489.0	60.6	40.0	0.53	< ~0.1
a-Si	-	-	-	473.0	77.0	-	0.00	-

Figure 2. An AFM Pictorial for samples grown by HWCVD.

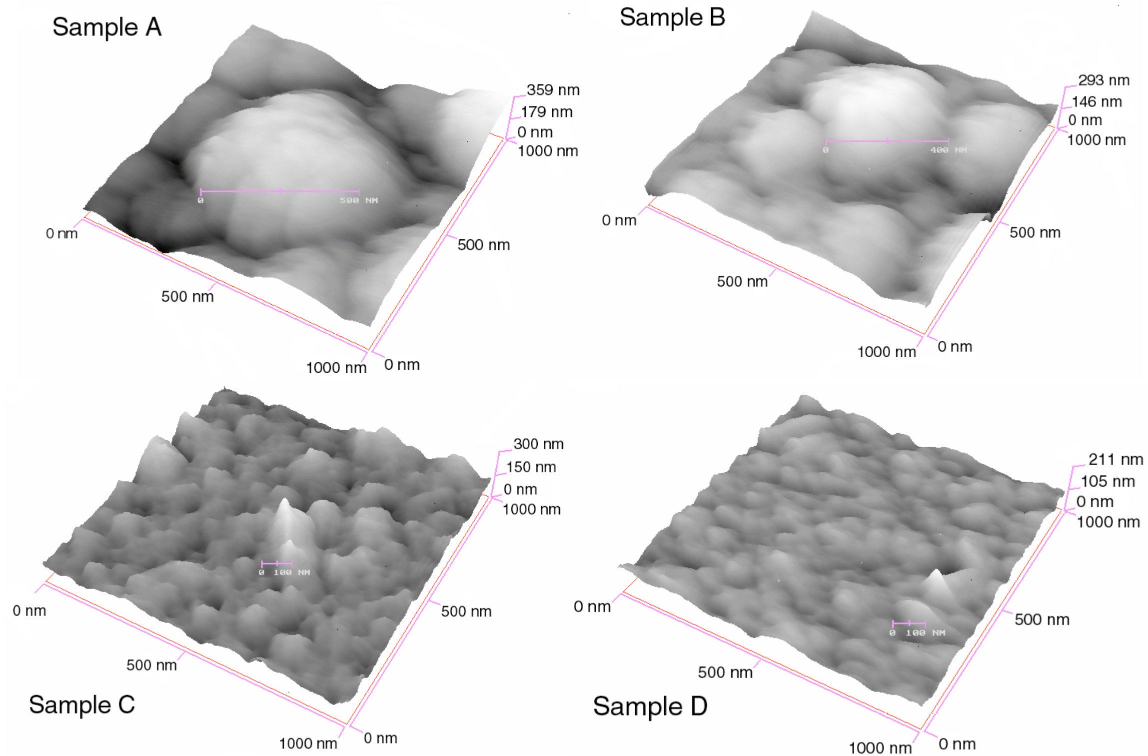

cause the absolute values of x_c to have a larger uncertainty. Therefore, for the best structural properties, the deposition conditions of Sample A are the ideal parameters for maximizing the grain size with the post-growth treatment for the four samples presented in this paper and the additional other samples studied.

In general, x ray diffraction data gathered for all samples showed l_c < average grain size (l_g) measured from AFM images. This indicates that the crystalline grains are aggregates of smaller crystallite material (~ .03 μm in average size). In samples receiving the post-growth treatment (Samples A and C), crystallites do not show a size increase on the same scale as the AFM feature size increase. This lack of correlation suggests that grain size increase measured by AFM is not due to the formation of larger crystallites, but rather it is due to the aggregation of crystallites.

A comparison of the x ray and Raman data shows that $l_d < l_c$. This result is important confirmation of the consistency of both of these values because it shows that the average length between defects is shorter than the distance between crystallite boundaries as it must be. Therefore, the all the measured lengths are in a self-consistent order, i.e. $l_d < l_c < l_g$. This self-consistency further confirms the validity of the data from all three characterization techniques.

CONCLUSIONS

We have shown that AFM, Raman spectroscopy, and x ray diffraction can be used to optimize HWCVD growth and post-growth annealing conditions to maximize grain size and crystalline volume fraction. The best results were obtained with a HWCVD process using SiF_4 along with SiH_4 and H_2 during deposition. In addition, it was shown that the trend of increasing x_c correlates with the trend of increasing grain size in our samples. Larger grains appear to be aggregates of smaller composite grains. These composite grains were found to also increase in size with the above deposition technique and post-growth annealing treatment.

These results indicate that use of SiF_4 during HWCVD growth and post-growth annealing could improve the performance of thin film silicon electronic devices such as thin film transistors (TFT) and solar cells.

ACKNOWLEDGMENTS

This work was supported by the National Renewable Energy Laboratory under subcontract number XAK-8-17619-13.

REFERENCES

1. G. Willeke, Physics and electronic properties of microcrystalline semiconductors, *Amorphous and Microcrystalline Semiconductor Devices*

Volume II Materials and Device Physics, ed. J. Kanicki (Artech House, N.Y., 1992) pp 55-80.
2. K. F. Feenstra, R. E. I. Schropp, and W. F. Van der Weg, J. Appl. Phy., **85**, 6843 (1999).
3. N. Wrysch, C. Droz, L. Feitknecht, M. Goerlitzer, U. Kroll, J. Meier, P. Torres, E. Vallat-Sauvain, A. Shah, and M. Vanecek, Mat. Res. Soc. Symp. Proc., **609**, 1 (2000).
4. D.L. Staebler and C.R. Wronski, Appl. Phys. Lett. **31**, 292 (1997).
5. Y. Chen and S. Wagner, Electrochemical Society Meeting Abstracts, **98-2,** 698 (The Electrochemical Society, Pennington, N.J., 1998).
6. E. C. Molenbroek, A. H. Mahan, and A. Gallagher, J. Appl. Phys., **82**, 1909 (1997).
7. H. Matsumura, Jpn. J. Appl. Phys. Part 1 **37**, 3175 (1998).
8. A. Heya, A Masuda, and H. Matsumura, Appl. Phys. Lett., **74**, 2143 (1999).
9. H. Kakinuma, M. Morhi, and T. Tsuroka, J. Appl. Phys., **77**, 646 (1995).
10. I. Kaiser, W. Fuhs, N. H. Nickel, and W. Pilz , Phys. Rev. B, **58**, 1718 (1998).
11. Y. Okada, J. Chen, I. H. Campbell, P. M. Fauchet, and S. Wagner, J. Appl. Phys., **67**, 1757 (1989).
12. E. Bardet, J. E. Bouree, M. Cuniot, J. Dixmier, P. Elkaim, J. Le Duigou, A. R. Middya, and J. Perrin, J. of Non-Cryst. Sol., **198-200**, 867 (1996).
13. H. Voutsas, M. K. Hatalis, J. Boyce, and A Chiang, J. Appl. Phys., **78**, 6999 (1995).
14. J. Gonzalez-Hernandez, G. H. Azarbayejani, R.Tsu, F.H. Pollak, Appl. Phys. Lett., **47**, 1350 (1985).
15. K. K. Tiong, M Amirtharaj, F. H. Pollak, and D. E. Aspnes, Appl. Phys. Lett., **44**, 122 (1984).